Spring 2022

Investigating the Main Protease (MPro) of SARS-CoV-2 as a Potential Drug Target

Valerie Giovina Pascetta
University of New Hampshire

Investigating the Main Protease (M^{Pro}) of SARS-CoV-2 as a Potential Drug Target

Valerie Pascetta

PI: Dr. Krisztina Varga

University of New Hampshire, Durham, NH

Biochemistry, Molecular, and Cellular Biology Honors Thesis

Topic: Spectroscopic Analysis of Viral Enzymatic Activity and Inhibition

Table of Contents

Abstract

The rapid spread of severe acute respiratory syndrome coronavirus 2 (SARS-CoV-2), the causative agent of the coronavirus disease 19 (COVID-19) pandemic has claimed the lives of roughly 6.2 million people worldwide as of May 2022. The virus's main protease (M^{pro}) has been identified as an attractive drug target due to the critical role it plays in the viral life cycle. The roughly 34 kDa M^{pro} cleaves functional viral polypeptides out of two long polyproteins at conserved cut sites, allowing them to fulfill their role in processes like transcription and replication. Here, we have studied the enzymatic activity and inhibition of M^{pro} and tested known (carmofur, ebselen, and tideglusib) and novel (CCG-50014, and CCG-203769) inhibitors using fluorescence spectroscopy. We report both the catalytic efficiency of M^{pro} (K_{cat} / K_M = 27,900 M^{-1} s^{-1} M^{-1} s^{-1}) and the IC_{50} values measured for tideglusib and ebselen (1.39 ± 0.2 µM and 0.40 ± 0.05 µM respectively) to be comparable to values published by Jin et *al*. [13]. We also report that the novel CCG-50014 has comparable IC_{50} value (1.39 ± 0.22 µM) to known inhibitors of this enzyme.

This work has been accepted for publication:

Jacob Andrzejczyk, Katarina Jovic, Logan M. Brown, Valerie G. Pascetta, Krisztina Varga, Harish Vashisth. Molecular Interactions and Inhibition of the SARS-CoV-2 Main Protease by a Thiadiazolidinone Derivative. *Accepted for publication.* ***Proteins*** *(2022)*

My contributions to this work: My contributions included working with Katarina Jovic under the supervision of Dr. Krisztina Varga to express and purify recombinant M^{Pro} and perform the inhibition assays with the five tested compounds. I also performed some preliminary activity assays with Katarina Jovic before Logan Brown collected the bulk of the data used to calculate catalytic efficiency. The computational studies were performed by Jacob Andrzejczyk under the supervision of Dr. Harish Vashisth.

Abbreviations: SARS, severe acute respiratory syndrome; MERS, Middle East respiratory syndrome; SARS-CoV-2, severe acute respiratory syndrome coronavirus 2; COVID-19, coronavirus disease 2019; ACE2, angiotensin-converting enzyme 2; nonstructural protein, nsp; ORF, open reading frame; main protease, M^{Pro}; thiadiazolidine, TDZD; regulators of G-protein signaling, RGS; inhibitory concentration, IC_{50}

Introduction

Coronaviruses are a large and diverse family of virus named for their unique crown-like spike proteins that cover the virion surface. These viruses are infectious to humans and animals and cause a variety of prevalent diseases with mild to severe symptoms. Coronavirus infections

typically manifest as moderate upper-respiratory tract illnesses [1]. However, the past two decades have seen coronavirus outbreaks with increasingly serious and fatal symptoms including severe acute respiratory syndrome (SARS) in 2002, Middle East respiratory syndrome (MERS) in 2012, and most notably, severe acute respiratory syndrome coronavirus 2 (SARS-CoV-2), the causative agent of coronavirus disease 2019 (COVID-19) [1, 2].

SARS-CoV-2 is a novel, β-coronavirus hypothesized to have zoonotic origins in bats [3] as well as pangolins [4]. Symptoms range from mild; fever, cough, shortness of breath, to severe; respiratory failure, pneumonia, and death. Outbreaks of the highly infectious COVID-19 virus were first reported in December of 2019 in Wuhan, China. The virus spread rapidly and, in March od 2020, a global pandemic was declared by the World Health Organization [3, 5]. The ongoing pandemic has claimed the lives of almost 6.2 million people worldwide as of May 2022 [6] and has sparked an international research effort to understand the molecular mechanisms of SARS-CoV-2 infection and develop effective treatments against its disease.

The virus is roughly 65-125 nm in diameter, and has a single stranded, positive sense, RNA genome. The genome encodes four main structural proteins (S,E,M and N) essential to host cell recognition and entry. The spike (S) protein is a transmembrane glycoprotein expressed on the viral surface which interacts with host lower respiratory cell angiotensin-converting enzyme 2 (ACE2) receptors. The envelope (E) protein plays a role in viral maturation. The membrane (M) protein determines viral envelope shape and assembly. The nucleocapsid (N) protein is an RNA binding protein that is involved in viral transcription, translation, and replication. The SARS-CoV-2 genome also encodes sixteen non-structural proteins (nsp 1-16) which have a variety of functions including suppression of the host immune response, cleavage of polyproteins, promotion of cytokine expression, and proofreading of the viral genome [3].

Once the S protein attaches to host cell ACE2 receptors, the membranes fuse and viral mRNA ready for translation enters the host cytoplasm. The genome contains fourteen open reading frames (ORFs) that encode both the structural and non-structural proteins. Among the first to be translated are the non-structural protein coding ORF1a and ORF1b which produce two long, overlapping polyproteins pp1a and pp1b. pp1a and pp1b are made up of the sixteen functional nsp polypeptides, including multiple proteins that aid in forming the polymerase and helicase complexes essential to viral transcription and replication. Enzymatic digestion of pp1a and pp1b is required to release the functional polypeptides from these larger polyproteins and allow them to participate in the viral life cycle. The nsp5 enzyme, also known as the main protease (M^{Pro}), is largely responsible for this digestion via its at least eleven conserved cut sites along the length of pp1a and pp1b, including its own autolytic cleavage [3].

M^{Pro} is a roughly 34 kDa, homodimeric enzyme comprised of 306 amino acids per monomer. Each monomer contains three subdomains, domains I and II (residues 8-101 and 102-184, respectively) are characterized by mainly β-barrel motifs, while domain III (residues 201-306) is primarily comprised of α-helices [7] (Fig. 1A). The M^{Pro} active site is situated at the interface of domains I and II and is comprised of key active site residues; M49, G143, H163, H164, E166, P168, Q189 and Y54, G143, H163 which form an oxyanion loop [8] (Fig. 1B). The M^{Pro} active site cleaves peptide bonds using a catalytic dyad (Fig. 1B) in which the -SH group of a cysteine residue (C145) donates a proton to the imidazole group of a histidine residue (H41) [9]. This allows for cleavage at the following recognition site sequences: L-Q ↓ (S, A, G) [10, 11].

Because of its pivotal role in the viral life cycle, high sequence conservation with other coronaviruses, and the lack of human homologues, M^{Pro} was identified as an attractive drug

target for the treatment of COVID-19. Although vaccine development has tremendously reduced the public health risks of COVID-19, the need for antiviral drugs to treat immunocompromised and un-vaccinated patients is still pressing, especially in the face of rapidly emerging variants. In December of 2021, the FDA announced its emergency authorization of Pfizer's Paxlovid, an M^{Pro} inhibitor and the first antiviral pill authorized to treat COVID-19 [12]. While the development of Paxlovid again marks a major achievement in combating the global COVID-19 pandemic, more research into antiviral development is still necessary to increase drug efficacy and reduce potential adverse side effects.

In this work we have investigated five potential small molecule M^{Pro} inhibitors, three of which are known M^{Pro} inhibitors (carmofur, tideglusib, and ebselen), and two that are novel (CCG-50014, and CCG-203769). The established inhibitors were pulled from a library of known compounds with applications that were initially unrelated to SARS-CoV-2. They were then repurposed and published in previous studies as effective M^{Pro} inhibitors [13, 14]. This study tested the three known inhibitors with the intent of replicating the results previously reported by Jin et *al.* [13] to optimize inhibition assay conditions and directly compare results with structurally similar inhibitors. The two novel inhibitors were selected based on structural similarity to tideglusib, a thiadiazolidine (TDZD) analog [15]. TDZD derivatives are known to covalently modify the cysteine residues of the regulator of G-protein signaling (RGS) proteins [16, 17, 18]. Because cysteine is an essential part of the M^{Pro} active site, it was hypothesized that novel TDZD derived inhibitors would demonstrate comparable levels of M^{Pro} inhibition to tideglusib. To investigate this hypothesis, recombinant M^{Pro} was expressed, and purified to test the inhibitory effects of the five ligands using fluorescence spectroscopy. These studies were used to complement molecular dynamics simulations for M^{Pro} inhibition [19].

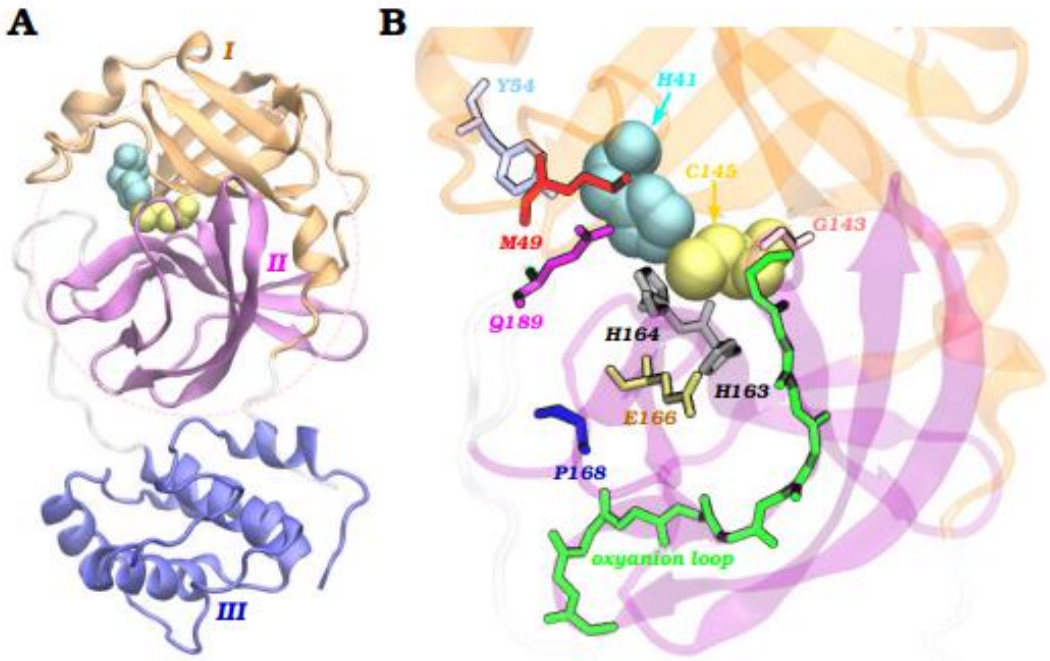

Figure 1: Structural details of M^{pro} monomer and active site. (A) M^{pro} monomer with domain I (orange), domain II (purple), and domain III (blue). Key catalytic residues H41 (cyan) and C145 (yellow) also pictured. (B) A zoomed view of the active site with key residues colored, labeled and shown in stick representations: M49 (red), G143 (pink), H163/H164 (gray), E166 (tan), P168 (blue), Q189 (purple), and the backbone atoms of residues that form the oxyanion loop (green). Figure was adapted from Padhi & Tripathi, 2021 [8].

Methods

M^{Pro} Expression and Purification

The expression vector, M^{Pro}-3C pET21b(+), containing the full-length SARS-CoV-2 gene encoding M^{Pro} (NC_045512) was purchased from GenScript, with the gene sequence optimized for expression in Escherichia coli. The final protein product contains four additional amino acids

(GPGG) before the C-terminal 6xHis-tag. Protein expression and purification procedures presented here were adopted and modified from Jin et. al [13]. The vector was transformed into *Escherichia coli* Rosetta-gami B(DE3) cells (EMD Millipore), which were grown for 5-6 hours in Luria-Bertani (LB) broth with 100 µg/mL ampicillin at 37 ˚C. Once the cells reached OD_{600} 0.7, the over expression of M^{Pro} was induced by adding 0.5 mM IPTG to the medium. After 11-12 hours of incubation at 16 ˚C, the liquid cell culture was centrifuged at 9,559 × *g* for 25 minutes (4 ˚C). The obtained *Escherichia coli* pellets were then stored -80 ˚C.

Protein purification started by thawing out a pellet at 4 ˚C for 30 minutes. Lysis buffer containing 20 mM Tris-HCl (pH 7.3), 150 mM NaCl, Halt™ Protease Inhibitor cocktail (Thermo Scientific) and Benzonase (EMD Millipore) were then added to the pellet. After 15-20 minutes of incubation with Lysis buffer, the cells were fully re-suspended and subjected to four rounds of mechanical cell lysis at 1,500 psi using the G-M French Press (Glen Mills). The cell lysate was then centrifuged at 20,217 × *g* for 30 minutes (4 ˚C). The obtained supernatant was filtered through 0.45- and 0.22-µm filters before purification. Since M^{Pro} was expressed with a C-terminal 6xHis-tag, the protein was purified using fast protein liquid chromatography system (FPLC; GE Healthcare AKTA purifier 900) equipped with a HisTrap FF 1 mL column. The protein was eluted from the column using an imidazole concentration gradient going up to 500 mM. The selected protein fractions were pooled, and imidazole was removed using Zeba™ spin desalting columns (following manufacturer's recommendation; Thermo Scientific). The sample was brought up to 5 mL prior to subjecting it to another round of Ni-affinity chromatography using a HisTrap HP 1 mL column. Upon collecting and pooling the selected fractions, the protein sample was exchanged into buffer containing 50 mM Tris-HCl and 1 mM EDTA (pH = 7.3) using Zeba™ spin desalting columns. The protein purity was assessed using SDS-PAGE. The

protein concentration was measured using JASCO V-650 UV-vis spectrophotometer. Upon determining the M^{Pro} purity and concentration, the protein identity was confirmed using LC-MS/MS mass spectrometry.

Activity and Inhibition Assays

Since it was previously shown that C-terminal 6His-tag does not alter M^{Pro} activity, the protease activity of uncleaved M^{Pro} containing the C-terminal 6His-tag was measured [20]. Both the activity and inhibition assays were performed following a modified protocol originally established by Jin et *al.* [13, 19] Fluorescence resonance energy transfer (FRET) peptide Mca-AVLQSGFRK(Dnp)K (GLBiochem) was used as the M^{Pro} substrate (excitation wavelength 325 nm, emission wavelength 392 nm). JASCO FP-8300 spectrofluorometer was used to measure the M^{Pro} activity. 1 µM M^{Pro} (final concentration) was mixed with varying concentrations of the peptide substrate (1.87 - 40 µM). Initial rates were obtained by fitting the linear portion of the curves to a straight line (typically around 35 - 50 seconds) (Kinetic Analysis, JASCO). K_M and V_{max} were calculated from the Lineweaver-Burk plot (1/V vs. 1/[S]) using Kinetic Analysis, JASCO. These values were used to determine the K_{cat} ($V_{max}/[M^{Pro}]$) as well as the catalytic efficiency (K_{cat}/K_M).

The degree of inhibition was measured for the three known M^{Pro} inhibitors [13, 14] carmofur (Fig. 3), tideglusib (Fig. 4) and ebselen (Fig. 5); and two novel ones, CCG-2203769 (Fig. 6) and CCG-50014 (Fig. 7). The inhibition assays were performed on a microplate reader SpectraMax Me (Molecular Devices). Similarly to the activity assays, fluorescence released the Mca-AVLQSGFRK(Dnp)K peptide cleavage by M^{Pro} was measured. Each reaction contained 0.2 µM M^{Pro}, 20 µM FRET peptide, varied inhibitor concentration (0.025 - 100 µM), and 5% DMSO in Assay buffer (50 mM Tris-HCl 1 mM EDTA pH 7.3). Data points were recorded every 4

seconds for 5 minutes, at 30 ˚C. SoftMax Pro 7 (Molecular Devices) was used to calculate the initial rates in units of relative fluorescence per second (RFU/s). The GraphPad Prism software was used to calculate the IC_{50} values and plot the inhibition curves.

Results/Discussion

Activity Assay

The activity assay was performed before testing inhibition to verify that the catalytic efficiency of M^{Pro} was comparable to the previously reported value by Jin et *al.* (K_{cat} / K_M = 28,500 M^{-1} s^{-1}) [13]. The Michaelis-Menten plot of [substrate] vs. RFU/min (Fig. 2) showed a Michaelis constant (K_M) of 7.88 μM ± 2.62 μM and a maximum rate (V_{max}) of 133.2 RFU/min. These values were then used to calculate the turnover number (K_{cat} = 2.10 s^{-1} ± 0.61 s^{-1}) and the catalytic efficiency (K_{cat} / K_M = 27,900 M^{-1} s^{-1} ± 6,250 M^{-1} s^{-1}) which was comparable to the value published by Jin et *al.* [13]. This confirmed that the IC_{50} values measured in the later inhibition assays could be objectively compared to the previously reported values by Jin et *al.* [13].

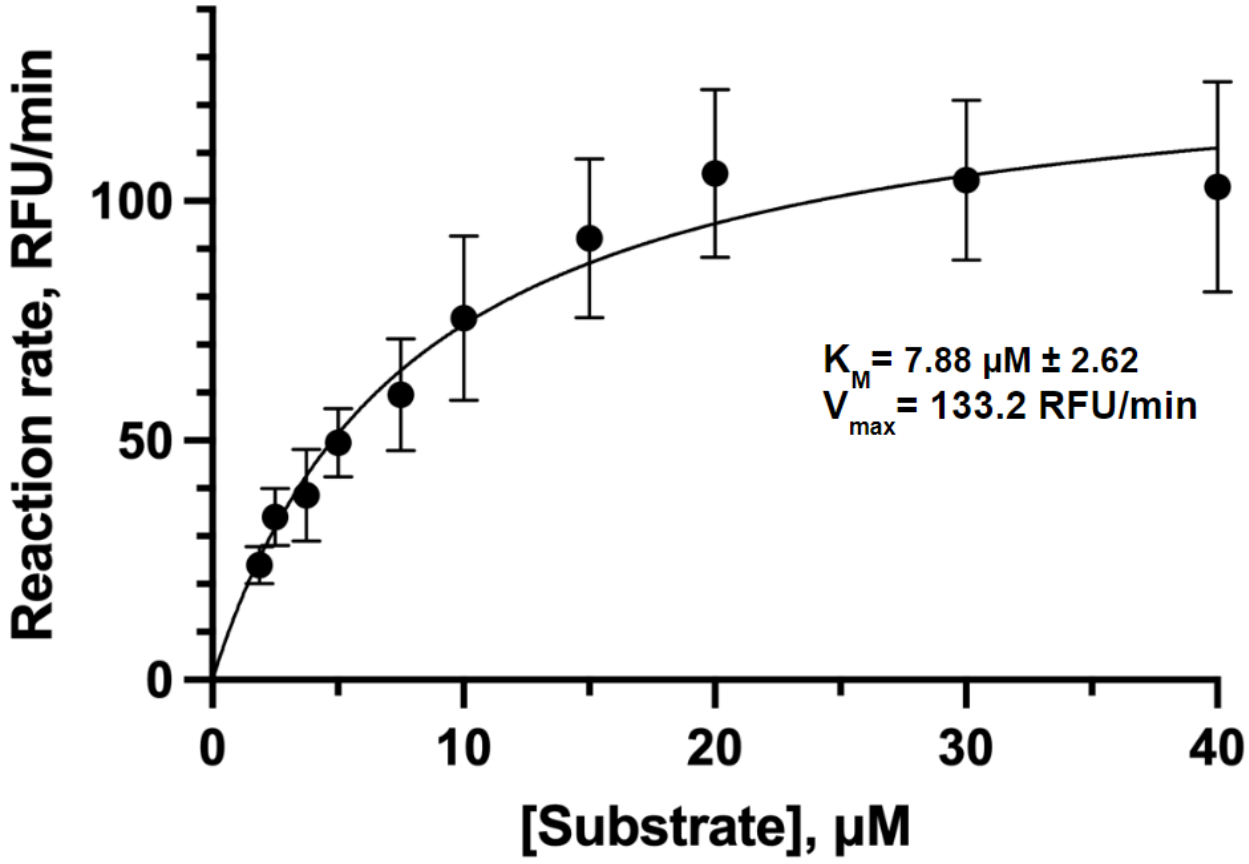

Figure 2: Michaelis-Menten plot showing hyperbolic M^{Pro} saturation. Plot shows [substrate] (uM) against reaction rate (RFU/min). Also shown is the K_M value with the error and V_{max} value.

Inhibition Assays

The inhibition data was analyzed using plots of normalized inhibition versus log [I]. Each inhibition plot exhibited a classic sigmoidal shape used to calculate the IC_{50} values. The IC_{50} values of the three known inhibitors, carmofur (Fig. 3), tideglusib (Fig. 4), and ebselen (Fig. 5) were calculated first for comparison with the values of Jin et *al.* [13]. The IC_{50} values of tideglusib (1.39 ± 0.2 µM) and ebselen (0.40 ± 0.05 µM) were comparable to reported values [13], while the IC_{50} value for carmofur (4.45 ± 0.52 µM) was approximately 2.5-fold higher, indicating that it may be a slightly weaker inhibitor of M^{pro} than previously reported. As our measured IC_{50} values were comparable to those previously reported [13], it was assumed that the inhibition assay could be used to reliably assess the potential of the two novel inhibitors and the results could be objectively compared to the IC_{50} values published by Jin et *al.*

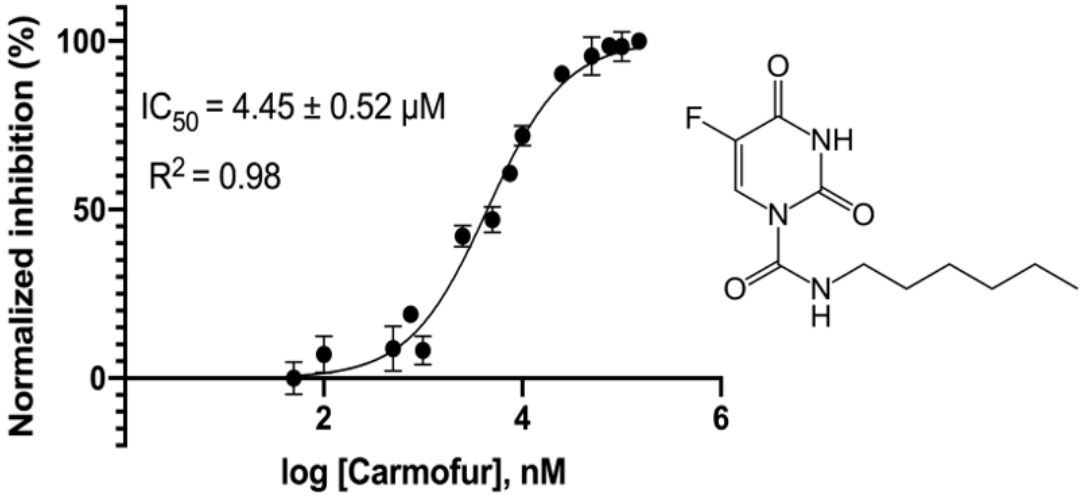

Figure 3: Normalized inhibition of M^{Pro} by carmofur (left) and carmofur chemical structure (right). Plot shows the normalized inhibition percentage of M^{Pro} (y-axis) against the log of the carmofur concentration (nM, x-axis). Also shown is the IC_{50} value with the error, and the proportion of variance value

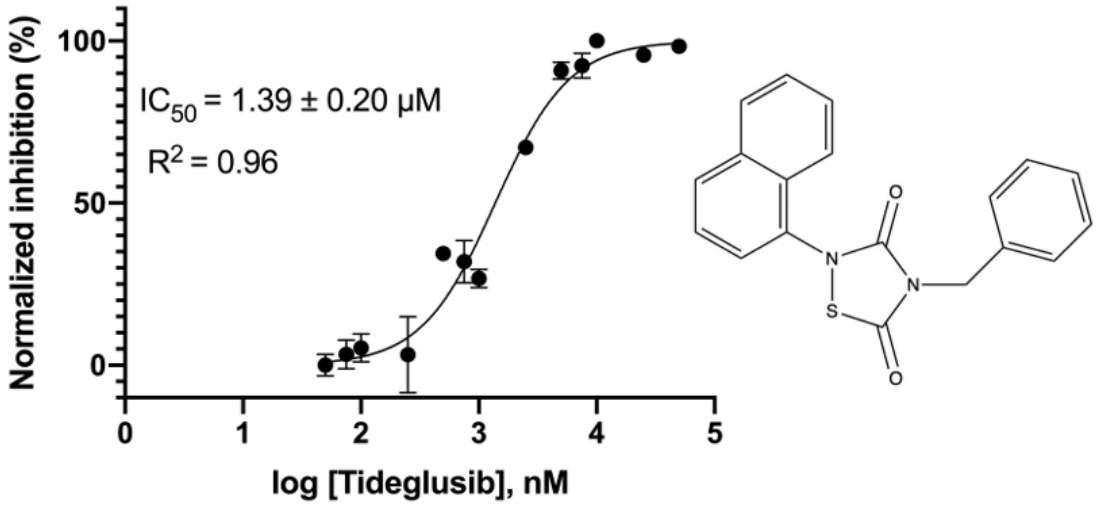

Figure 4: Normalized inhibition of M^{Pro} by tideglusib (left) and tideglusib chemical structure (right). Plot shows the normalized inhibition percentage of M^{Pro} (y-axis) against the log of the tideglusib concentration (nM, x-axis). Also shown is the IC_{50} value with the error, and the proportion of variance value.

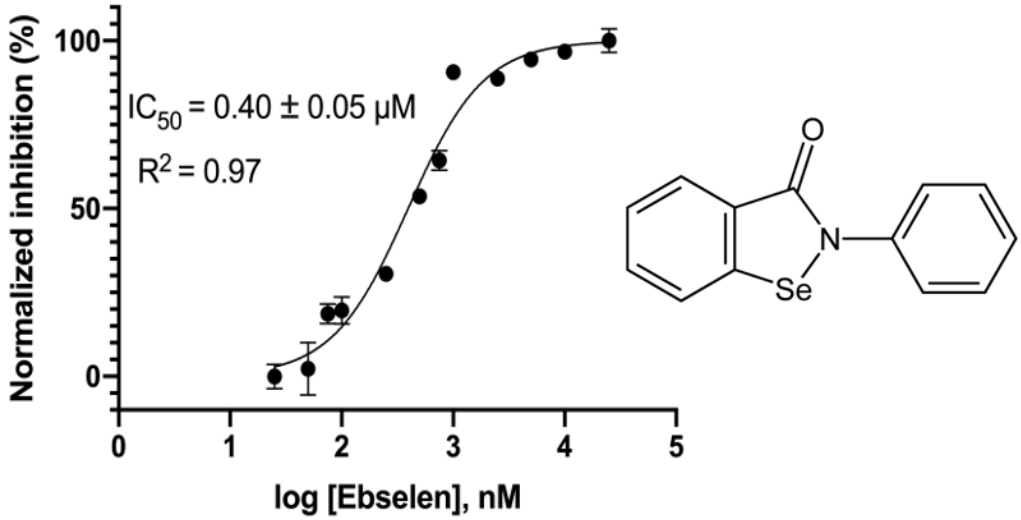

Figure 5: Normalized inhibition of M^{Pro} by ebselen (left) and ebselen chemical structure (right). Plot shows the normalized inhibition percentage of M^{Pro} (y-axis) against the log of the ebselen concentration (nM, x-axis). Also shown is the IC_{50} value with the error, and the proportion of variance value.

The IC_{50} values of the two novel inhibitors; CCG-50014 and CCG-203769 were then calculated using the same normalized inhibition vs log [I] plots. The IC_{50} value of CCG-50014 was 1.39 ± 0.22 µM (Fig. 6); thus CCG-50014 exhibited inhibition comparable to that tideglusib, as hypothesized. These results are promising for CCG-50014's potential application as an M^{Pro} inhibitor. The IC_{50} value calculated for CCG-203769 was 10.95 ± 1.74 µM (Fig. 7). Because this value was higher than CCG-50014 and all the known inhibitors, the compound showed less potential as an M^{Pro} inhibitor.

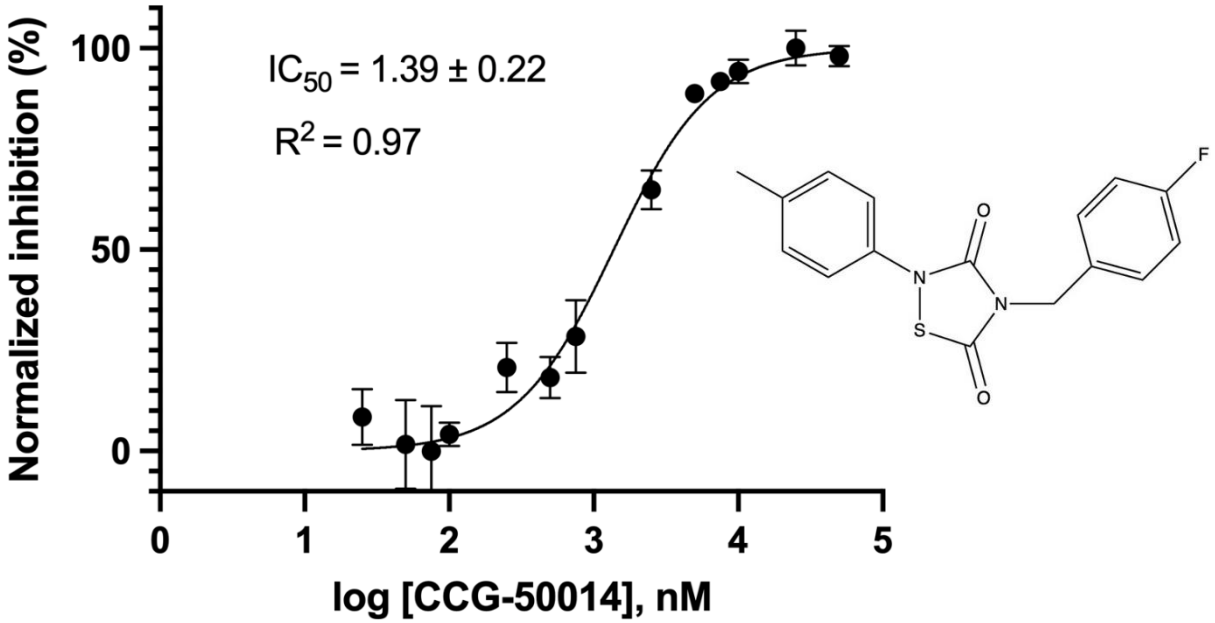

Figure 6: Normalized inhibition of M^{Pro} by CCG-50014 (left) and CCG-50014 chemical structure (right). Plot shows the normalized inhibition percentage of M^{Pro} (y-axis) against the log of the CCG-50014 concentration (nM, x-axis). Also shown is the IC_{50} value with the error, and the proportion of variance value.

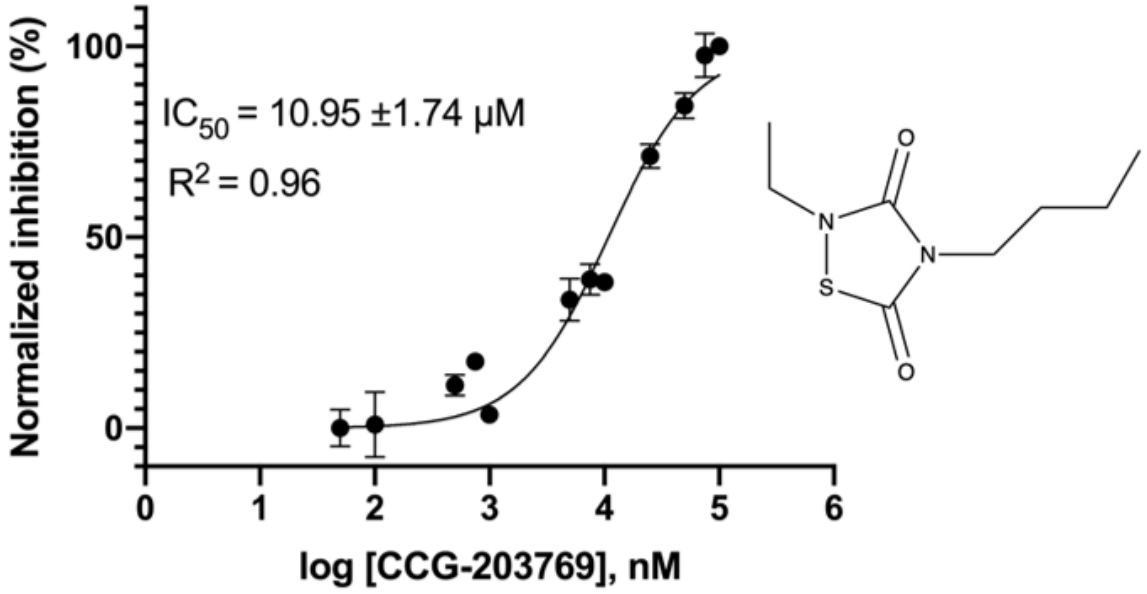

Figure 7: Normalized inhibition of M^{Pro} by CCG-203769 (left) and CCG-203769 chemical structure (right). Plot shows the normalized inhibition percentage of M^{Pro} (y-axis) against the log of the CCG-203769 concentration (nM, x-axis). Also shown is the IC_{50} value with the error, and the proportion of variance value.

The difference in inhibition between CCG-50014 and CCG-203769 was attributed to the different moieties attached to each structure's thiazole ring. Where CCG-203769 has aliphatic moieties attached to its central thiazole ring (an ethyl and a butyl group Fig. 7), CCG-50015 has aromatic moieties attached (a methylbenzene and a fluorophenyl group Fig. 6). The molecular dynamics studies (by the Vashisth group) complementary to this work showed these aromatic moieties to be a stabilizing feature of CCG-50014's interaction with the M^{Pro} active site. The active site residues located closest to the fluorophenyl side chain were shown to be stabilized in the presence of covalently-bound CCG-50014 through several stacking interactions and hydrogen bonds. While the active site residues that showed increased fluctuations in the presence

of CCG-5001 were those residues that did not have direct interactions with its aromatic side-chains [19].

Conclusions

In this work we have investigated inhibitory the potential of three known M^{Pro} inhibitors: carmofur, tideglusib, and ebselen, and two novel M^{Pro} inhibitors: CCG-50014 and CCG-203769 using fluorescence spectroscopy assays. Both the catalytic efficiency of M^{pro} (K_{cat} / K_M = 27,900 M^{-1} s^{-1} ± 6,250 M^{-1} s^{-1}) and the IC_{50} values measured for tideglusib and ebselen (1.39 ± 0.2 µM and 0.40 ± 0.05 µM respectively) are comparable to the values reported by Jin et *al*. [13]. The IC_{50} value measured for carmofur (4.45 ± 0.52 µM) indicated it is a less potent M^{Pro} inhibitor than previously reported [13]. The IC_{50} value measured for CCG-50014 (1.39 ± 0.22 µM) was comparable to those of tideglusib, while the value for CCG-203769 (10.95 ± 1.74 µM) signified it is a less potent inhibitor of M^{Pro}.

Molecular dynamics simulations revealed this difference to be because of the moieties attached to each structure's central thiazole ring. While CCG-50014 has aromatic moieties attached, CCG-203769 has aliphatic moieties. The simulations showed these aromatic moieties to have several stabilizing interactions with the key residues of the active site.

Acknowledgements

This work was supported by the National Institutes of Health (NIH) under grant R35GM138217 (H. V.) and by the Collaborative Research Excellence (CoRE) program at the University of New Hampshire (UNH). Additional support was also provided by the UNH Center of Integrated Biomedical and Bioengineering Research (CIBBR) core facilities through a grant from NIH (P20GM113131). The content is solely the responsibility of the authors and does not necessarily represent the official views of the NIH. Support for the computational studies was provided through the following resources: Premise, a central shared high-performance computing cluster at UNH supported by the Research Computing Center and Biomade, a heterogeneous CPU/GPU cluster supported by the NSF EPSCoR award (OIA-1757371). This work also acknowledges and thanks Dr. Richard R. Neubig, Professor of Pharmacology and Toxicology at Michigan State University, for providing the inhibitor CCG-50014 and CCG-203769, and Dr. Douglas E. Frantz, Professor of Chemistry at University of Texas at San Antonio, for providing the three inhibitors tideglusib, ebselen, and carmofur.

I would also like to thank the members of the Varga group at the University of New Hampshire for their support throughout this research, and special thanks to Katarina Jovic for her excellent mentorship, leadership, and hard work throughout this project.

References

[1] National Institute of Allergy and Infectious Diseases. (2022, March). *Coronaviruses*. National Institute of Allergy and Infectious Diseases. Retrieved April 10, 2022, from https://www.niaid.nih.gov/diseases-conditions/coronaviruses

[2] Ye, Z.-W., Yuan, S., Yuen, K.-S., Fung, S.-Y., Chan, C.-P., & Jin, D.-Y. (2020). Zoonotic origins of human Coronaviruses. *International Journal of Biological Sciences*, *16*(10), 1686–1697. https://doi.org/10.7150/ijbs.45472

[3] Astuti, I., & Ysrafil. (2020). Severe acute respiratory syndrome coronavirus 2 (SARS-COV-2): An overview of viral structure and host response. *Diabetes & Metabolic Syndrome: Clinical Research & Reviews*, *14*(4), 407–412. https://doi.org/10.1016/j.dsx.2020.04.020

[4] Zhang, T., Wu, Q., & Zhang, Z. (2020). Probable pangolin origin of SARS-COV-2 associated with the COVID-19 outbreak. *Current Biology*, *30*(7). https://doi.org/10.1016/j.cub.2020.03.022

[5] Cucinotta D, Vanelli M. (2020). WHO Declares COVID-19 a Pandemic. *Acta Biomed*, 91(1):157-160. doi: 10.23750/abm.v91i1.9397.

[6] World Health Organization. (2022). *WHO coronavirus (COVID-19) dashboard*. World Health Organization. Retrieved April 10, 2022, from https://covid19.who.int/

[7] Khan, S. A., Zia, K., Ashraf, S., Uddin, R., & Ul-Haq, Z. (2020). Identification of chymotrypsin-like protease inhibitors of SARS-COV-2 *via* integrated computational approach. *Journal of Biomolecular Structure and Dynamics*, *39*(7), 2607–2616. https://doi.org/10.1080/07391102.2020.1751298

[8] Padhi, A. K., & Tripathi, T. (2021). Targeted design of drug binding sites in the main protease of SARS-COV-2 reveals potential signatures of adaptation. *Biochemical and Biophysical Research Communications*, *555*, 147–153. https://doi.org/10.1016/j.bbrc.2021.03.118

[9] Keillor, J. W., & Brown, R. S. (1992). Attack of zwitterionic ammonium thiolates on a distorted anilide as a model for the acylation of papain by amides. A simple demonstration of a bell-shaped ph/rate profile. *Journal of the American Chemical Society*, *114*(21), 7983–7989. https://doi.org/10.1021/ja00047a004

[10] He, J., Hu, L., Huang, X., Wang, C., Zhang, Z., Wang, Y., Zhang, D., & Ye, W. (2020). Potential of coronavirus 3c-like protease inhibitors for the development of new anti-SARS-cov-2 drugs: Insights from structures of protease and inhibitors. *International Journal of Antimicrobial Agents*, *56*(2), 106055. https://doi.org/10.1016/j.ijantimicag.2020.106055

[11] Li, Q., & Kang, C. B. (2020). Progress in developing inhibitors of SARS-COV-2 3c-like protease. *Microorganisms*, *8*(8), 1250. https://doi.org/10.3390/microorganisms8081250

[12] U.S. Food and Drug Administration. (2021). *Coronavirus (COVID-19) update: FDA authorizes first oral antiviral for treatment of covid-19*. U.S. Food and Drug Administration. Retrieved April 11, 2022, from https://www.fda.gov/news-events/press-announcements/coronavirus-covid-19-update-fda-authorizes-first-oral-antiviral-treatment-covid-19

[13] Jin, Z., Du, X., Xu, Y., Deng, Y., Liu, M., Zhao, Y., Zhang, B., Li, X., Zhang, L., Peng, C., Duan, Y., Yu, J., Wang, L., Yang, K., Liu, F., Jiang, R., Yang, X., You, T., Liu, X., … Yang, H. (2020). Structure of mpro from SARS-COV-2 and discovery of its inhibitors. *Nature*, *582*(7811), 289–293. https://doi.org/10.1038/s41586-020-2223-y

[14] Ma, C., Hu, Y., Townsend, J. A., Lagarias, P. I., Marty, M. T., Kolocouris, A., & Wang, J. (2020). Ebselen, disulfiram, Carmofur, PX-12, Tideglusib, and Shikonin are nonspecific promiscuous SARS-COV-2 main protease inhibitors. *ACS Pharmacology & Translational Science*, *3*(6), 1265–1277. https://doi.org/10.1021/acsptsci.0c00130

[15] Balasubramaniam, M., Mainali, N., Bowroju, S. K., Atluri, P., Penthala, N. R., Ayyadevera, S., Crooks, P. A., & Shmookler Reis, R. J. (2020). Structural modeling of gsk3β implicates the inactive (DFG-out) conformation as the target bound by TDZD analogs. *Scientific Reports*, *10*(1). https://doi.org/10.1038/s41598-020-75020-w

[16] Liu, Y., & Vashisth, H. (2021). Allosteric pathways originating at cysteine residues in regulators of G-protein signaling proteins. *Biophysical Journal*, *120*(3), 517–526. https://doi.org/10.1016/j.bpj.2020.12.010

[17] Shaw, V. S., Mohammadiarani, H., Vashisth, H., & Neubig, R. R. (2018). Differential protein dynamics of regulators of G-protein signaling: Role in specificity of small-molecule inhibitors. *Journal of the American Chemical Society*, *140*(9), 3454–3460. https://doi.org/10.1021/jacs.7b13778

[18] Vashisth, H., Storaska, A. J., Neubig, R. R., & Brooks, C. L. (2013). Conformational dynamics of a regulator of G-protein signaling protein reveals a mechanism of allosteric inhibition by a small molecule. *ACS Chemical Biology*, *8*(12), 2778–2784. https://doi.org/10.1021/cb400568g

[19] Andrzejczyk, J., Jovic, K., Brown, L. M., Pascetta, V. G., Varga, K., & Vashisth, H. (2022). Molecular Interactions and Inhibition of the SARS-CoV-2 Main Protease by a Thiadiazolidinone Derivative. *Submitted and under review*.

[20] Sacco, M. D., Ma, C., Lagarias, P., Gao, A., Townsend, J. A., Meng, X., Dube, P., Zhang, X., Hu, Y., Kitamura, N., Hurst, B., Tarbet, B., Marty, M. T., Kolocouris, A., Xiang, Y., Chen, Y., & Wang, J. (2020). Structure and inhibition of the SARS-COV-2 main protease reveal strategy for developing dual inhibitors against M pro and cathepsin L. *Science Advances*, *6*(50). https://doi.org/10.1126/sciadv.abe0751

[21] Nelson, D. L., & Cox, M. M. (2017). *Lehninger principles of biochemistry* (7th ed.). W.H. Freeman.

[22] Pang Y, Gordon R. Optical trapping of a single protein. Nano Lett. 2012 Jan 11;12(1):402-6. doi: 10.1021/nl203719v. Epub 2011 Dec 16. PMID: 22171921.

[23] Moy, R. H.; Gold, B.; Molleston, J. M.; Schad, V.; Yanger, K.; Salzano, M.-V.; Yagi, Y.; Fitzgerald, K. A.; Stanger, B. Z.; Soldan, S. S.; et al. Antiviral autophagy restricts rift valley fever virus infection and is conserved from flies to mammals. *Immunity* **2014**, *40* (1), 51–65 DOI: 10.1016/j.immuni.2013.10.020.

[24] Billecocq Agnès; Spiegel, M.; Vialat, P.; Kohl, A.; Weber, F.; Bouloy Michèle; Haller, O. NSS protein of Rift Valley fever virus blocks interferon production by inhibiting host gene transcription. *Journal of Virology* **2004**, *78* (18), 9798–9806 DOI: 10.1128/jvi.78.18.9798-9806.2004.